

Dynamic Pre-training: Towards Efficient and Scalable All-in-One Image Restoration

Akshay Dudhane¹ Omkar Thawakar¹ Syed Waqas Zamir²
 Salman Khan^{1,3} Fahad Shahbaz Khan^{1,4} Ming-Hsuan Yang^{5,6,7}

¹Mohamed bin Zayed University of AI ²Inception Institute of AI
³Australian National University ⁴Linköping University
⁵University of California, Merced ⁶Yonsei University ⁷Google Research

Abstract. All-in-one image restoration tackles different types of degradations with a unified model instead of having task-specific, non-generic models for each degradation. The requirement to tackle multiple degradations using the same model can lead to high-complexity designs with fixed configuration that lack the adaptability to more efficient alternatives. We propose DyNet, a dynamic family of networks designed in an encoder-decoder style for all-in-one image restoration tasks. Our DyNet can seamlessly switch between its bulkier and lightweight variants, thereby offering flexibility for efficient model deployment with a single round of training. This seamless switching is enabled by our weights-sharing mechanism, forming the core of our architecture and facilitating the reuse of initialized module weights. Further, to establish robust weights initialization, we introduce a dynamic pre-training strategy that trains variants of the proposed DyNet concurrently, thereby achieving a 50% reduction in GPU hours. To tackle the unavailability of large-scale dataset required in pre-training, we curate a high-quality, high-resolution image dataset named Million-IRD having 2M image samples. We validate our DyNet for image denoising, deraining, and dehazing in all-in-one setting, achieving state-of-the-art results with 31.34% reduction in GFlops and a 56.75% reduction in parameters compared to baseline models. The source codes and trained models are available at <https://github.com/akshaydudhane16/DyNet>.

Keywords: All-in-one · Image Restoration · Foundation model

1 Introduction

The image restoration (IR) task seeks to improve low-quality input images. Despite several advancements in IR, diverse degradation types and severity levels present in images continue to pose a significant challenge. The majority of existing methods [3, 8, 13–15, 31, 46, 47, 52] learn image priors implicitly, requiring separate network training for different degradation types, levels, and datasets. Further, these methods require a prior knowledge of image degradation for effective model selection during testing, thereby lacking generality to cater diverse degradations.

All-in-one restoration aims to restore images with an unknown degradation using a single *unified* model. Recent advancements, such as AirNet [26] and PromptIR [36], have addressed the all-in-one restoration challenge by employing contrastive learning and implicit visual prompting techniques, respectively. Specifically, the state-of-the-art PromptIR [36] employs an implicit prompting to learn degradation-aware prompts on the decoder side, aiming to refine the decoder features. This approach, while intriguing, does not extend to the refinement of encoder features, which are left unprocessed. Despite the interesting idea of implicit prompting, it poses a considerable challenge for deployment due to its poor computational efficiency with 37M parameters and 243 GFlops to process a single 224×224 sized image. The practical application of such models is therefore challenging due to the high computational requirements, especially in resource-constraint hand-held devices. However, choosing lightweight models invariably leads to a trade-off between accuracy and efficiency [28, 56]. Most of these models aim to reduce parameter counts by strided convolutions and feature channel splitting [22, 23, 28]. Some strategies also operate within the frequency domain to reduce the computational demands linked to attention mechanisms [62] or non-local operations [18] while few methods like [9, 49] partition the feature space for efficient processing, or split the attention across dimensions to improve the computational efficiency [9, 61].

Towards optimizing all-in-one IR efficiency without sacrificing performance, in this paper, we introduce a novel weights-sharing mechanism. In this scheme, the weights of a network module are shared with its subsequent modules in a series. This approach substantially reduces the number of parameters, resulting in a more streamlined network architecture. We deploy the proposed weights-sharing mechanism in an encoder-decoder style architecture named Dynamic Network (DyNet). Apart from the computational efficiency, the proposed DyNet provides exceptional flexibility as by merely changing the module weights reuse frequency, one can easily adjust the network depth and correspondingly switch between its bulkier and light-weight variants *during training*.

While DyNet offers great adaptability with orders of speedup, a common challenge with lightweight networks is the potential compromise on overall accuracy. To counteract this, we show that a large-scale pre-training strategy can effectively improve the performance of our lightweight models. By initializing the network with weights derived from the pre-training, the model benefits from a strong foundation, which can lead to enhanced performance even with a reduced parameter count. However, large-scale pre-training is computationally intensive and requires significant GPU hours. Therefore, we introduce an efficient and potent dynamic pre-training strategy capable of training both bulkier and lightweight network variants within a single pre-training session, thereby achieving significant savings of 50% in GPU hours. Complementing this, we have compiled a comprehensive, high-quality, high-resolution dataset termed Million-IRD, consisting of 2 million image samples. Our main contributions are as follows:

- We propose DyNet, a dynamic family of networks for all-in-one image restoration tasks. DyNet offers easy switching between its bulkier and light-weight

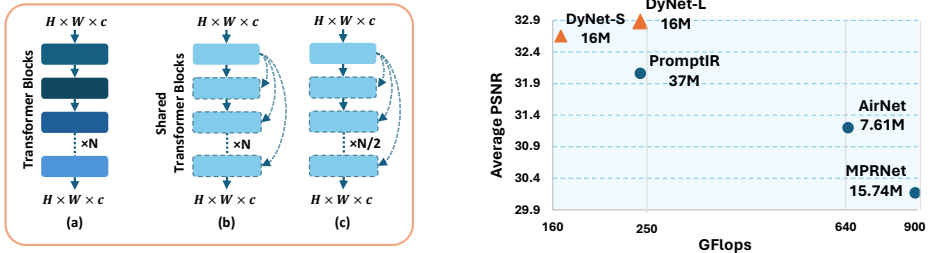


Fig. 1: Left: At any given encoder-decoder level, (a) Series of transformer blocks in existing PromptIR [36], (b) The proposed transformer block weights sharing mechanism in our DyNet-L. We initialize one transformer block at each encoder-decoder level and shared its weights with the subsequent N transformer blocks. (c) Our lightweight variant DyNet-S. Here, the number of transformer blocks are halved and weights of the first transformer block are shared with $N/2$ subsequent transformer blocks. **Right:** A plot of average PSNR in All-in-one restoration setting vs GFlops and parameters (in millions). The proposed DyNet-S achieves boost of 0.59 dB with 31.34% reduction in GFlops and a 56.75% reduction in parameters compared to the baseline PromptIR [36].

variants. This flexibility is made possible through a weight-sharing strategy, which is the central idea of our network design, allowing for the efficient reuse of initialized module weights.

- We introduce a Dynamic Pre-training strategy, a new approach that allows the concurrent large-scale pre-training of both bulkier and light-weight network variants within a single session. This innovative strategy reduces GPU hours significantly by 50%, addressing the pressing challenge of resource-intensive model pre-training on a large-scale.
- We curate a comprehensive pre-training dataset comprising 2 million high-quality, high-resolution, meticulously filtered images. From this dataset, we extract 8 million non-overlapping high-resolution patches, each sized 512×512 , utilized for the pre-training of variants of the proposed DyNet.

Through the synergy of these techniques, our proposed DyNet achieves an average gain of 0.82 dB for image de-noising, deraining, and dehazing within an all-in-one setting, with 31.34% reduction in GFlops and a 56.75% reduction in network parameters compared to the baseline; refer Fig. 1.

2 Related Work

Image restoration seeks to restore images from their degraded low-quality versions, with the restoration process varying considerably across different tasks. Research in image restoration has predominantly concentrated on addressing single degradation challenges [11, 34, 38, 40, 45, 52, 53, 58, 60]. Although significant progress has been made in single degradation restoration techniques, research in multi-degradation restoration using a unified model is still relatively under-explored. Multi-degradation restoration, however, provides more practical

advantages as the information about input degradation type is not required to select the task-specific model and it also enhances model storage efficiency over single-degradation restoration.

The critical challenge in multi-task image restoration is developing a single model capable of addressing various types of degradation and precisely restoring low-quality images. The IPT model [7], for instance, relies on prior knowledge of the corruption affecting the input image, utilizing a pre-trained transformer backbone equipped with distinct encoders and decoder heads tailored for multi-task restoration. However, in blind image restoration, we do not have such prior information about the degradation. In this direction, Li *et al.* [26] propose a unified network for multiple tasks such as denoising, deraining, and dehazing, employing an image encoder refined through contrastive learning. However, it requires a two-stage training process, where the outcome of contrastive learning relies on selecting positive and negative pairs and the availability of large data samples. Further, motivated by easy implementation and broad applicability of prompts, PromptIR [36] introduces a concept where degradation-aware prompts are learned implicitly within an encoder-decoder architecture for all-in-one image restoration. PromptIR applies implicit prompting to the decoder side to refine the decoder features. However, it does not extend to the refinement of encoder features, which are left unprocessed.

Although the above-discussed methods tackle multi-task image restoration, they suffer from low efficiency due to a large number of parameters and substantial GFlops consumption. Consequently, deploying these models in environments where efficiency is crucial factor becomes difficult due to their demanding computational needs. However, opting for lightweight models introduces an inevitable accuracy-efficiency trade-off [56]. The primary cause is that many current methods focus on reducing parameter counts through techniques like strided convolutions and feature channel splitting [22, 23, 28]. Additionally, few approaches work within the frequency domain to reduce the computational burden associated with attention mechanisms [62] or non-local operations [18]. Furthermore, methods like [9, 49] partition the feature space for efficient processing, while [9, 61] split the attention across dimensions to improve the computational efficiency. In contrast, our proposed approach focuses on an efficient and scalable all-in-one image restoration model that incorporates a module weights-sharing mechanism. We demonstrate that strategic fundamental adjustments to the network architecture result in substantial performance improvements.

3 Proposed Approach

Existing state-of-the-art all-in-one image restoration (IR) approaches incur a high computational footprint and do not provide the flexibility to support models with variable depths during training. Towards more accurate, but lightweight and flexible architecture design for all-in-one IR, this work proposes a Dynamic Network Architecture (Sec. 3.1) and a Dynamic Pretraining Strategy (Sec. 3.2).

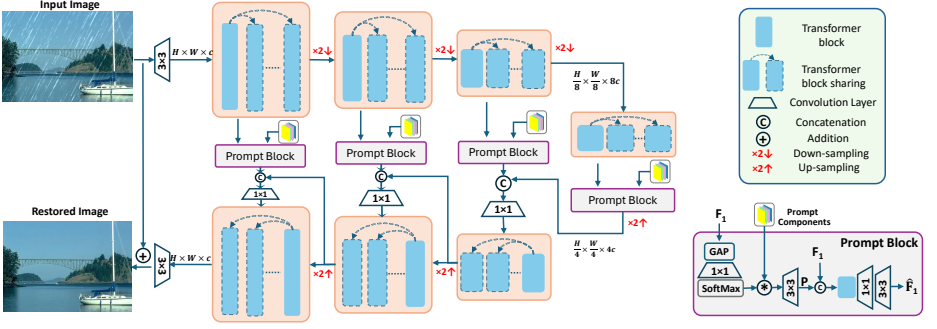


Fig. 2: The overall pipeline of the proposed Dynamic Network (DyNet) for all-in-one image restoration. DyNet enhances a low-quality input image using a four-level encoder-decoder architecture. A distinctive aspect of DyNet lies in its weight-sharing strategy: at each level, the initial transformer block’s weights are sequentially passed to subsequent blocks, significantly reducing the network’s parameters and enhancing its flexibility. This approach allows for easy modification of DyNet’s complexity, toggling between more bulkier or lightweight variants by adjusting the frequency of weight sharing among the blocks at each encoder-decoder level. Moreover, we maintain the encoder-decoder feature consistency by implicitly learning degradation-aware prompts at skip connections rather than on the decoder side as in PromptIR [36].

3.1 Dynamic Network (DyNet) Architecture

Our lightweight architecture is based on a novel weight-sharing mechanism for IR models. This mechanism allows the network module’s weights to be reused across subsequent modules in sequence, thereby significantly reducing the total number of parameters and leading to a more efficient network structure. We implement this weight-sharing approach within an encoder-decoder style architecture, which we term the Dynamic Network (DyNet). Within DyNet, at each encoder-decoder level, module weights are shared across a pre-specified number of subsequent modules. This not only enhances computational efficiency but also grants remarkable flexibility to the architecture. By simply altering the frequency of weight sharing, users can easily modify the network’s depth, seamlessly transitioning between bulkier or lightweight variants of DyNet.

Overall Pipeline. The overall pipeline of the proposed DyNet is shown in Fig. 2. The proposed DyNet begins by extracting low-level features $\mathbf{F}_0 \in \mathbb{R}^{H \times W \times C}$ from a given degraded input image $\mathbf{I} \in \mathbb{R}^{H \times W \times 3}$ through a convolution operation. Subsequently, the feature embedding undergoes a 4-level hierarchical encoder-decoder, gradually transforming into deep latent features $\mathbf{F}_l \in \mathbb{R}^{\frac{H}{8} \times \frac{W}{8} \times 8C}$. We utilize the existing Restormer’s [52] Transformer block as a fundamental feature extraction module. For every level of the encoder and decoder, we initialize the weights for a first transformer block, which are subsequently reused across the subsequent blocks in a series up to the specified frequency at that level. For example, at a given encoder/decoder level, w^1 denotes weights of the first

transformer block, we can define the output \mathbf{F}_{out} of that encoder/decoder level, given input features \mathbf{F}_{in} as,

$$\begin{aligned}\mathbf{F}_{out} &= w^1(\mathbf{F}_{in}) && \text{for } b = 1 \\ \mathbf{F}_{out} &= \bigcirc_{b=2:f} w^b(\mathbf{F}_{out}) && \text{for } b = 2 : f\end{aligned}$$

where, \bigcirc represents a self loop, iterate for $b=2:f$; $w^b = w^1$ for $b = 2, 3, \dots, f$. Here, f denotes the module weights reuse frequency for a given encoder or decoder level.

We gradually increase the reuse frequency of the transformer block from the top level to the bottom level, thereby increasing the network depth. The multi-level encoder systematically reduces spatial resolution while increasing channel capacity, facilitating the progressive extraction of low-resolution latent features from a high-resolution input image. Subsequently, the multi-level decoder gradually restores the high-resolution output from these low-resolution latent features. To enhance the decoding process, we integrate prompt blocks [36], which learn degradation-aware prompts implicitly through the prompt generation module (PGM) followed by the prompt-interaction module (PIM). Unlike the existing PromptIR [36], our approach incorporates degradation-aware implicit prompt blocks at skip connections. This implicit prompting via skip connections enables the transfer of degradation-aware encoder features to the decoder side, thereby enhancing the restoration process. This fundamental correction in the network design gives us significant improvement for all-in-one image restoration tasks, as detailed in the experimental section (Sec. 5).

Architectural details. At each encoder-decoder level, by simply changing the module weights reuse frequency (f), we obtain DyNet’s bulky and lightweight variants. Fig. 2 shows the core architecture of our DyNet. At each encoder-decoder level, we initialize weights (w^1) for the first transformer block [52] and reuse them for the subsequent blocks. We vary the reuse frequency at each encoder-decoder level and obtain our bulkier and lightweight variants. DyNet comprises four encoder-decoder levels, with the bulky variant (DyNet-L) employing reuse frequencies of $f = [4, 6, 6, 8]$ at encoder-decoder level 1 to level 4, respectively. In contrast, the lightweight variant (DyNet-S) applies weights reuse frequencies $f = [2, 3, 3, 4]$ for encoder-decoder level 1 to level 4, respectively. Further, we incorporate a prompt block [36] at each skip connection, which enhances the encoder features being transferred to the decoder from the encoder. Overall, there are three prompt blocks deployed at each level, each consisting of five prompt components.

3.2 Dynamic Pre-training Strategy

In recent times, large-scale pre-training has become a key strategy to improve given network performance. Initializing the network with pre-trained weights

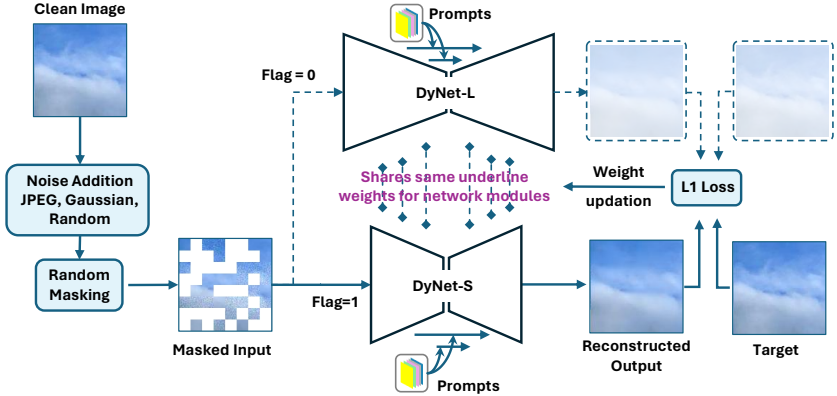


Fig. 3: The proposed dynamic pre-training strategy is shown. Given a clean image, we create a degraded version by injecting noise (Gaussian or Random), JPEG artifacts and random masking within the same image. Two variants (small and large) of our DyNet are then trained in parallel branches to reconstruct the clean image from masked degraded inputs. Notably, the weights are shared between both variants (DyNet-S and DyNet-L) since they are based on the same architecture but with an intra-network weight-sharing scheme with varying frequencies of block repetition. One of the two parallel branches is randomly activated in a single forward pass of the model (Flag being the binary indicator variable to show branch activation). The dotted lines show the network path is inactivated (Flag=0). An L1 loss is used to calculate pixel differences between reconstructed outputs and targets to update the shared weights of both branches. Both the inter and intra-model weight-sharing as well as random activation of branches lead to a significant reduction in GPU hours required for pre-training.

provides a robust foundation, boosting performance even with fewer parameters. However, this strategy is resource-intensive, demanding considerable computational power and GPU hours. Therefore, we propose a dynamic pre-training that is capable of simultaneous training of multiple variants of the network. These networks are unified by shared network modules weight but varying network depth. This strategy enables the concurrent training of a diverse set of models tailored to various computational needs and task complexities, all while leveraging a shared baseline architecture. Through the proposed dynamic pre-training strategy, we train both DyNet-L and DyNet-S versions of our DyNet concurrently in a single training session, achieving a 50% reduction in GPU hours.

DyNet-L and DyNet-S utilize the same underlying weights for the transformer blocks initialized at each encoder-decoder level. They just differ in the reuse frequency of these initialized transformer blocks at each encoder-decoder level. Thus, during training iterations, we randomly alternate between DyNet-L and DyNet-S ensuring the optimization of the shared underlying weights as shown in Fig. 3. Moreover, we improve the generalization capability of our DyNet variants by adopting an input masking strategy akin to that proposed in masked auto-encoders [19]. We randomly mask portions of an image and train the DyNet

variants to reconstruct these masked regions in a self-supervised fashion. The dataset used for this training is described below.

4 Million-IRD: A Dataset for Image Restoration

Large-scale pre-training for image restoration effectively demands large-scale, high-quality and high-resolution datasets. The current image restoration datasets [2, 27, 35], when combined, offer only a few thousand images. This is considerably inadequate compared to the extensively large-scale datasets [41, 42] utilized in pre-training for other high-level tasks, such as visual recognition, object detection, and segmentation. The relatively small size of the existing training sets for image restoration restricts the performance capabilities of the underlying networks. More importantly, we are motivated by the scaling laws in high-level tasks that demonstrate the large-scale pre-training can enable even lightweight, efficient model designs to reach the performance mark of much heavier models [1]. To address this gap, we introduce a new million-scale dataset named *Million-IRD* having $\sim 2M$ high-quality, high-resolution images, curated specifically for the pre-training of models for image restoration tasks. Examples from our *Million-IRD* dataset are shown in the Fig. 4. Our data collection and pre-processing pipeline are discussed below.

4.1 Data collection and Pre-processing

We combine the existing high-quality, high-resolution natural image datasets such as LSDIR [27], DIV2K [2], Flickr2K [35], and NTIRE [4]. Collectively these datasets have 90K images having spatial size ranging between $< 1024^2, 4096^2 >$. Apart from these datasets, existing Laion-HR [42] dataset has 170M unfiltered high-resolution images of average spatial size 1024^2 . However, these 170M samples are not directly suitable for model pre-training due to the predominant presence of low-quality images. Examples of such low-quality images are illustrated in Fig. 4 (on right side). Therefore, we focus on filtering out only high-quality images by discarding those of low quality. Given the impracticality of manual sorting of 170M images, we employ various image quality metrics NIQE [33], BRISQUE [32], and NIMA [43]. Only images surpassing certain pre-defined thresholds T_{NIQE} , $T_{BRISQUE}$, and T_{NIMA} are selected; we empirically define thresholds for these metrics. With the mutual consensus of these metrics, we effectively filter out low-quality images having poor textural details, excessive flat areas, various artifacts like blur and noise, or unnatural content. By processing nearly 100M images in the Laion-HR dataset [42], we sort out 2M high-quality images having spatial resolution of 1024^2 , or above. Examples of these high-quality filtered images are presented in the Fig. 4 (on left side).

4.2 Data post-processing

Overall, our Million-IRD dataset has 2.09 million high-quality, high-resolution images. Each image in our dataset comes with metadata detailing its down-

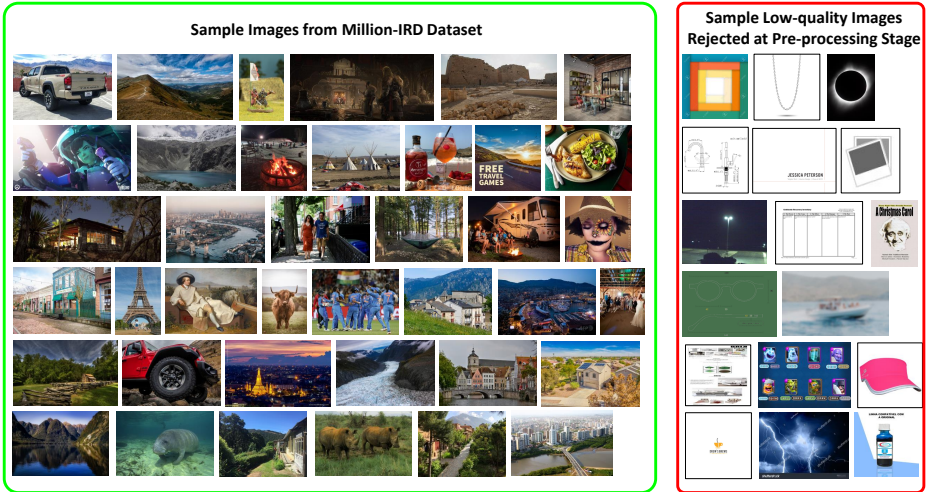


Fig. 4: On the left: Sample images from our Million-IRD dataset, which features a diverse collection of high-quality, high-resolution photographs. This includes a variety of textures, scenes from nature, sports activities, images taken during the day and at night, intricate textures, wildlife, shots captured from both close and distant perspectives, forest scenes, pictures of monuments, etc. **On the right:** Sample low-quality images filtered out during the data pre-processing phase (Sec. 4.1). These images were excluded due to being blurry, watermarked, predominantly featuring flat regions, representing e-commerce product photos, or being noisy or corrupted from artifacts.

load link and the image resolution. A detailed breakdown of images and their respective sources is provided in the supplementary material. We extract high-resolution non-overlapping patches (of spatial size 512^2) from each image, followed by the application of a flat region detector which eliminates any patch comprising more than 50% flat area. This post-processing phase allows us to assemble a pool of ~ 8 million diverse image patches, tailored for the pre-training phase of our DyNet variants.

5 Experiments

We validate the proposed DyNet across three key image restoration tasks: de-hazing, deraining, and denoising. In line with the existing PromptIR [36], our experiments are conducted under two distinct setups: (a) All-in-One, wherein a single model is trained to handle all three degradation types, and (b) Single-task, where individual models are trained for each specific image restoration task.

5.1 Implementation Details

Dynamic Pre-training. For robust weights initialization, we conduct a dynamic pre-training for two variants of our DyNet, i.e., DyNet-L and DyNet-S.

Both variants share the same underline weights but differ in their transformer block reuse frequency at each encoder-decoder level. For the encoder-decoder levels 1 to 4, we set transformer block weights reuse frequencies of [4,6,6,8] for DyNet-L and [2,3,3,4] for DyNet-S. We use all $\sim 8\text{M}$ patches of size 512^2 from our Million-IRD dataset for the dynamic pre-training. We randomly crop a 128^2 region from each patch, employing a batch size of 32. Each of these cropped patches undergoes a random augmentation to 50% of its area using either JPEG compression, Gaussian noise, or random noise with varying levels. Furthermore, we mask 30% of the patch, leaving the remaining portion unaltered. In total, 80% of the input patch undergoes modification, either through degradation or masking. For weight optimization, we use the L1 loss and Adam optimizer with parameters $\beta_1 = 0.9$ and $\beta_2 = 0.999$, setting the learning rate to $1\text{e-}4$ for 1 million iterations. Using the setup described above, we simultaneously pre-train both DyNet-L and DyNet-S. At any given iteration, we randomly switch between the two variants. Intriguingly, with each iteration, the shared underlying weights are optimized as shown in Fig. 3. As a result, by the end of this single pre-training session, we get DyNet-L and DyNet-S sharing the same trained underlying weights but differ in network depth, making them suitable for various challenges, including robustness and efficiency.

Datasets. For all-in-one and single-task implementations, we follow the same training protocol as existing PromptIR [36] and finetune the pre-trained DyNet-S and DyNet-L. Following [26, 36], we prepare datasets for various restoration tasks. Specifically, for image denoising, we combine the BSD400 [5] (400 training images) and WED [29] (4,744 images) datasets, adding Gaussian noise at levels $\sigma \in 15, 25, 50$ to create noisy images. Testing is conducted on the BSD68 [30] and Urban100 [20] datasets. For deraining, we use Rain100L [50] with 200 training and 100 testing clean-rainy image pairs. Dehazing employs the SOTS [25] dataset, featuring 72,135 training and 500 testing images. To develop a unified model for all tasks, we merge these datasets, fine-tune pre-trained DyNet-L and DyNet-S for 120 epochs and directly evaluate them across different tasks. While, for a single task, the pre-trained DyNet-L is fine-tuned for 120 epochs on a respective training set of the task.

5.2 Comparisons on multiple degradations under All-in-one setting

We benchmark our DyNet against a range of general image restoration models [12, 17, 44, 54] and specific all-in-one solutions [16, 26, 36], as shown in Table 1. On average, across various tasks, DyNet-L and DyNet-S outperform the previously best PromptIR [36] by 0.82 dB and 0.59 dB, respectively, with DyNet-S also cutting down on 56.75% of parameters and 31.34% of GFlops. For image denoising, DyNet-S achieves a 1.09 dB higher average PSNR compared to DL [16], with Fig. 5 showcasing its ability to deliver noise-free images with improved structural integrity. Notably, DyNet-L sets a new benchmark in image deraining and dehazing with improvements of 2.34 dB and 1.4 dB in PSNR, respectively. Visual comparisons in Fig. 6 and 7 demonstrate DyNet’s superior capability

Table 1: Comparison results in the All-in-one restoration setting. Our DyNet-L model outperforms PromptIR [36] by 0.82 dB on average across tasks. Additionally, our DyNet-S model achieves a 0.59 dB average improvement over PromptIR [36], with reductions of 31.34% in parameters and 56.75% in GFlops.

Comparative Methods	Dehazing		Deraining		Denoising on BSD68 dataset [30])			Average
	on SOTS [25]	on Rain100L [16]			$\sigma = 15$	$\sigma = 25$	$\sigma = 50$	
BRDNet [44]	23.23/0.895	27.42/0.895	32.26/0.898	29.76/0.836	26.34/0.836			27.80/0.843
LPNet [17]	20.84/0.828	24.88/0.784	26.47/0.778	24.77/0.748	21.26/0.552			23.64/0.738
FDGAN [12]	24.71/0.924	29.89/0.933	30.25/0.910	28.81/0.868	26.43/0.776			28.02/0.883
MPRNet [54]	25.28/0.954	33.57/0.954	33.54/0.927	30.89/0.880	27.56/0.779			30.17/0.899
DL [16]	26.92/0.391	32.62/0.931	33.05/0.914	30.41/0.861	26.90/0.740			29.98/0.875
AirNet [26]	27.94/0.962	34.90/0.967	33.92/0.933	31.26/0.888	28.00/0.797			31.20/0.910
PromptIR [36]	30.58/0.974	36.37/0.972	33.98/0.933	31.31/0.888	28.06/0.799			32.06/0.913
DyNet-S (Ours)	31.51/0.980	38.11/0.981	34.06/0.935	31.41/0.891	28.15/0.802			32.65/0.918
DyNet-L (Ours)	31.98/0.981	38.71/0.983	34.11/0.936	31.44/0.892	28.18/0.803			32.88/0.920

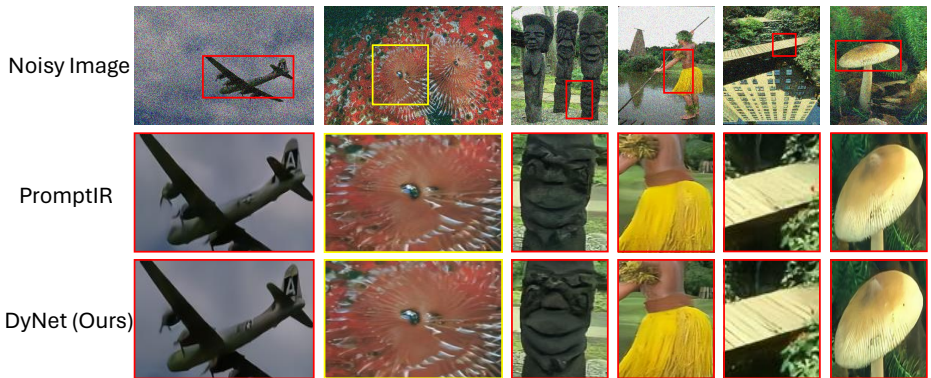


Fig. 5: Comparative analysis of image denoising by all-in-one methods on the BSD68 dataset [30]. Our DyNet-L reduces noise, producing more sharp and clear image compared to the PromptIR [36].

Table 2: Dehazing results in the single-task setting on the SOTS benchmark dataset [25]. Our DyNet-L achieves a boost of 0.76 dB over PromptIR [26].

DehazeNet [6]	MSCNN [39]	AODNet [24]	EPDN [37]	FDGAN [12]	AirNet [26]	Restormer [52]	PromptIR [36]	DyNet-L
22.46/0.851	22.06/0.908	20.29/0.877	22.57/0.863	23.15/0.921	23.18/0.900	30.87/0.969	31.31/0.973	32.07/0.982

in removing rain and haze, respectively, producing more cleaner images than PromptIR [36].

5.3 Comparisons on single degradation

We assess DyNet-L’s efficacy in single-task settings, where distinct models are tailored to specific restoration tasks, demonstrating the effectiveness of content-adaptive prompting through prompt blocks. Our results, as shown in Table 2,

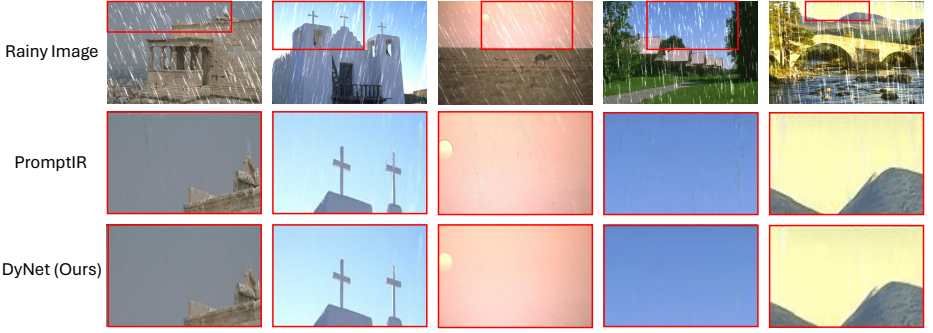


Fig. 6: Comparative analysis of image deraining by all-in-one methods on the Rain100L dataset [16]. Our DyNet-L successfully eliminates rain streaks, producing clear, rain-free images as compared to the recent PromptIR [36].

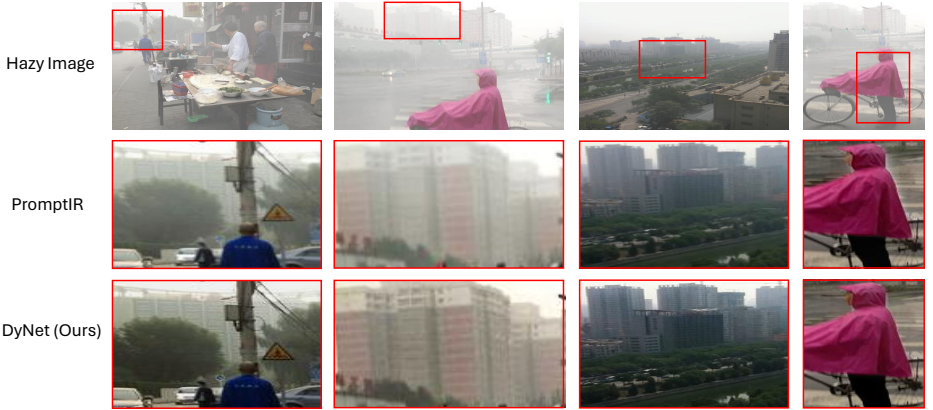


Fig. 7: Comparative analysis of image dehazing by all-in-one methods on the SOTS dataset [25]. Our approach reduces haze, producing more clear image compared to the PromptIR [36].

Table 3: Deraining results in the single-task setting on Rain100L [16]. Compared to the PromptIR [36], our method yields 1.68 dB PSNR improvement.

DIDMDN [55]	UMR [51]	SIRR [48]	MSPFN [21]	LPNet [17]	AirNet [26]	Restormer [52]	PromptIR	DyNet-L
23.79/0.773	32.39/0.921	32.37/0.926	33.50/0.948	33.61/0.958	34.90/0.977	36.74/0.978	37.04/0.979	38.85/0.984

indicate DyNet-L’s superior performance with an improvement of 0.76 dB over PromptIR [36] and 1.2 dB over Restormer [52] in dehazing. This pattern is consistent across other tasks, including deraining and denoising. Notably, compared to PromptIR [36], DyNet-L achieves performance gains of 1.81 dB in deraining (refer to Table 3) and achieves a 0.13 dB improvement in denoising at a noise level of $\sigma = 50$ on the Urban100 dataset (Table 4).

Table 4: Denoising comparisons in the single-task setting on BSD68 [30] and Urban100 [20] datasets. For the challenging noise level of $\sigma = 50$ on Urban100 [20], our DyNet-L obtains 0.64 dB gain compared to AirNet [26].

Comparative Methods	BSD68 [30]			Urban100 [20]		
	$\sigma = 15$	$\sigma = 25$	$\sigma = 50$	$\sigma = 15$	$\sigma = 25$	$\sigma = 50$
CBM3D [10]	33.50/0.922	30.69/0.868	27.36/0.763	33.93/0.941	31.36/0.909	27.93/0.840
DnCNN [57]	33.89/0.930	31.23/0.883	27.92/0.789	32.98/0.931	30.81/0.902	27.59/0.833
IRCNN [58]	33.87/0.929	31.18/0.882	27.88/0.790	27.59/0.833	31.20/0.909	27.70/0.840
FFDNet [59]	33.87/0.929	31.21/0.882	27.96/0.789	33.83/0.942	31.40/0.912	28.05/0.848
BRDNet [44]	34.10/0.929	31.43/0.885	28.16/0.794	34.42/0.946	31.99/0.919	28.56/0.858
AirNet [26]	34.14/0.936	31.48/0.893	28.23/0.806	34.40/0.949	32.10/0.924	28.88/0.871
Restormer [52]	34.29/0.937	31.64/0.895	28.41/0.810	34.67/0.969	32.41/0.927	29.31/0.878
PromptIR [36]	34.34/0.938	31.71/0.897	28.49/0.813	34.77/0.952	32.49/0.929	29.39/0.881
DyNet-L (Ours)	34.40/0.938	31.76/0.897	28.53/0.813	34.84/0.952	32.60/0.930	29.52/0.882

Table 5: Ablation experiments for different variants of the proposed DyNet.

Comparative Methods	Dehazing on SOTS [25]	Deraining on Rain100L [16]	Denoising on BSD68 dataset [30])			Average	Par GFlops
			$\sigma = 15$	$\sigma = 25$	$\sigma = 50$		
PromptIR [36]	30.58/0.974	36.37/0.972	33.98/0.933	31.31/0.888	28.06/0.799	32.06/0.913	37M 242.355
(a) Results without masked dynamic pre-training on Million-IRD							
DyNet-S	30.10/0.976	37.10/0.975	33.94/0.931	31.28/0.880	28.03/0.789	32.09/0.910	16M 166.38
DyNet-L	30.67/0.977	37.68/0.975	33.97/0.933	31.31/0.889	28.04/0.797	32.33/0.914	16M 242.35
(b) Results with masked dynamic pre-training on Million-IRD							
DyNet-S	31.51/0.980	38.11/0.981	34.06/0.935	31.41/0.891	28.15/0.802	32.65/0.918	16M 166.38
DyNet-L	31.98/0.981	38.71/0.983	34.11/0.936	31.44/0.892	28.18/0.803	32.88/0.920	16M 242.35

5.4 Ablation studies

To study the impact of different components, we conduct various ablation experiments in the all-in-one setting, as summarized in Table 5. Table 5(a) illustrates that our DyNet-L and DyNet-S achieves comparable performance to the baseline PromptIR [36] with reductions of 56.75% in parameters and 31.34% in GFlops, without the proposed dynamic pre-training on Million-IRD dataset. This shows that the proposed fundamental correction of placing prompt block at skip connections is effective compared to on the decoder side as given in PromptIR [36]. Furthermore, pre-training on our Million-IRD dataset brings a significant improvement, resulting in an average PSNR increase of 0.55 dB for DyNet-L compared to the DyNet-L without pre-training as shown in Table 5(b). A similar effect is observed for our DyNet-S variant. Moreover, our proposed dynamic training strategy reduces GPU hours by 50% when training variants of the DyNet. Overall, each of our contributions (*i.e.*, implicit prompting via skip connections, dynamic network architecture, Million-IRD dataset, and dynamic pre-training strategy) synergistically enhances the performance of the proposed approach, while significantly reducing GFlops and learning parameters compared to the baseline PromptIR [36].

Table 6: Performance of the proposed DyNet-S on different combinations of degradation types i.e., removal of noise, rain, and haze.

Degradation			Denoising on BSD68 dataset [30]			Deraining on Rain100L [16]	Dehazing on SOTS [25]
Noise	Rain	Haze	$\sigma = 15$	$\sigma = 25$	$\sigma = 50$		
✓	✗	✗	34.30/0.938	31.65/0.897	28.42/0.813	-	-
✗	✓	✗	-	-	-	38.72/0.984	-
✗	✗	✓	-	-	-	-	31.45/0.980
✓	✓	✗	34.19/0.936	31.54/0.894	28.30/0.808	38.61/0.984	-
✓	✗	✓	34.11/0.935	31.45/0.893	28.18/0.802	-	31.69/0.981
✗	✓	✓	-	-	-	38.16/0.982	31.55/0.980
✓	✓	✓	34.06/0.935	31.41/0.891	28.15/0.802	38.11/0.981	31.51/0.980

Training model with different combinations of degradation. In Table 6, we compare the performance of our DyNet-S in all-in-one setting on aggregated datasets, assessing how varying combinations of degradation types affect it’s effectiveness. All the models in this ablation study are trained for 80 epochs. Here in Table 6, we assess how varying combinations of degradation types (tasks) influence the performance of our DyNet. Notably, the DyNet trained for a combination of the derain and de-noise tasks exhibits better performance for image deraining than the DyNet trained on the combination of derain and dehaze. This shows that some degradations are more relevant for the model to benefit from when trained in a joint manner.

6 Conclusion

This paper introduces a novel weight-sharing mechanism within the Dynamic Network (DyNet) for efficient all-in-one image restoration tasks, significantly improving computational efficiency with a performance boost. By adjusting module weight-reuse frequency, DyNet allows for seamless alternation between bulkier and lightweight models. The proposed dynamic pre-training strategy simultaneously trains bulkier and lightweight models in a single training session. Thus saving 50% GPU hours compared to traditional training strategy. The ablation study shows that the accuracy of both bulky and lightweight models significantly boosts with the proposed dynamic large-scale pre-training on our Million-IRD dataset. Overall, our DyNet significantly improves the all-in-one image restoration performance with a 31.34% reduction in GFlops and a 56.75% reduction in parameters compared to the baseline models.

References

1. Abnar, S., Dehghani, M., Neyshabur, B., Sedghi, H.: Exploring the limits of large scale pre-training. arXiv:2110.02095 (2021)
2. Agustsson, E., Timofte, R.: Ntire 2017 challenge on single image super-resolution: Dataset and study. In: CVPR Workshops (2017)

3. Alghallabi, W., Dudhane, A., Zamir, W., Khan, S., Khan, F.S.: Accelerated mri reconstruction via dynamic deformable alignment based transformer. In: WMLMI (2023)
4. Ancuti, C.O., Ancuti, C., Vasluianu, F.A., Timofte, R.: Ntire 2021 nonhomogeneous dehazing challenge report. In: CVPR (2021)
5. Arbelaez, P., Maire, M., Fowlkes, C., Malik, J.: Contour detection and hierarchical image segmentation. TPAMI (2011)
6. Cai, B., Xu, X., Jia, K., Qing, C., Tao, D.: Dehazenet: An end-to-end system for single image haze removal. TIP (2016)
7. Chen, H., Wang, Y., Guo, T., Xu, C., Deng, Y., Liu, Z., Ma, S., Xu, C., Xu, C., Gao, W.: Pre-trained image processing transformer. In: CVPR (2021)
8. Chen, L., Chu, X., Zhang, X., Sun, J.: Simple baselines for image restoration. In: ECCV (2022)
9. Cui, Y., Knoll, A.: Psnet: Towards efficient image restoration with self-attention. IEEE RAL (2023)
10. Dabov, K., Foi, A., Katkovnik, V., Egiazarian, K.: Color image denoising via sparse 3d collaborative filtering with grouping constraint in luminance-chrominance space. In: ICIP (2007)
11. Dong, H., Pan, J., Xiang, L., Hu, Z., Zhang, X., Wang, F., Yang, M.H.: Multi-scale boosted dehazing network with dense feature fusion. In: CVPR (2020)
12. Dong, Y., Liu, Y., Zhang, H., Chen, S., Qiao, Y.: Fd-gan: Generative adversarial networks with fusion-discriminator for single image dehazing. In: AAAI (2020)
13. Dudhane, A., Biradar, K.M., Patil, P.W., Hambarde, P., Murala, S.: Varicolored image de-hazing. In: CVPR (2020)
14. Dudhane, A., Zamir, S.W., Khan, S., Khan, F.S., Yang, M.H.: Burst image restoration and enhancement. In: CVPR (2022)
15. Dudhane, A., Zamir, S.W., Khan, S., Khan, F.S., Yang, M.H.: Burstormer: Burst image restoration and enhancement transformer. In: CVPR (2023)
16. Fan, Q., Chen, D., Yuan, L., Hua, G., Yu, N., Chen, B.: A general decoupled learning framework for parameterized image operators. TPAMI (2019)
17. Gao, H., Tao, X., Shen, X., Jia, J.: Dynamic scene deblurring with parameter selective sharing and nested skip connections. In: CVPR (2019)
18. Guo, L., Zha, Z., Ravishankar, S., Wen, B.: Self-convolution: A highly-efficient operator for non-local image restoration. In: ICASSP (2021)
19. He, K., Chen, X., Xie, S., Li, Y., Dollár, P., Girshick, R.: Masked autoencoders are scalable vision learners. In: CVPR (2022)
20. Huang, J.B., Singh, A., Ahuja, N.: Single image super-resolution from transformed self-exemplars. In: CVPR (2015)
21. Jiang, K., Wang, Z., Yi, P., Chen, C., Huang, B., Luo, Y., Ma, J., Jiang, J.: Multi-scale progressive fusion network for single image deraining. In: CVPR (2020)
22. Kligvasser, I., Shaham, T.R., Michaeli, T.: xunit: Learning a spatial activation function for efficient image restoration. In: CVPR (2018)
23. Kong, F., Li, M., Liu, S., Liu, D., He, J., Bai, Y., Chen, F., Fu, L.: Residual local feature network for efficient super-resolution. In: CVPR (2022)
24. Li, B., Peng, X., Wang, Z., Xu, J., Feng, D.: Aod-net: All-in-one dehazing network. In: ICCV (2017)
25. Li, B., Ren, W., Fu, D., Tao, D., Feng, D., Zeng, W., Wang, Z.: Benchmarking single-image dehazing and beyond. TIP (2018)
26. Li, B., Liu, X., Hu, P., Wu, Z., Lv, J., Peng, X.: All-in-one image restoration for unknown corruption. In: CVPR (2022)

27. Li, Y., Zhang, K., Liang, J., Cao, J., Liu, C., Gong, R., Zhang, Y., Tang, H., Liu, Y., Demandolx, D., et al.: Lsdire: A large scale dataset for image restoration. In: CVPR (2023)
28. Li, Y., Zhang, Y., Timofte, R., Van Gool, L., Yu, L., Li, Y., Li, X., Jiang, T., Wu, Q., Han, M., et al.: Ntire 2023 challenge on efficient super-resolution: Methods and results. In: CVPR (2023)
29. Ma, K., Duanmu, Z., Wu, Q., Wang, Z., Yong, H., Li, H., Zhang, L.: Waterloo exploration database: New challenges for image quality assessment models. TIP (2016)
30. Martin, D., Fowlkes, C., Tal, D., Malik, J.: A database of human segmented natural images and its application to evaluating segmentation algorithms and measuring ecological statistics. In: ICCV (2001)
31. Mehta, N., Dudhane, A., Murala, S., Zamir, S.W., Khan, S., Khan, F.S.: Gated multi-resolution transfer network for burst restoration and enhancement. In: CVPR (2023)
32. Mittal, A., Moorthy, A.K., Bovik, A.C.: No-reference image quality assessment in the spatial domain. TIP (2012)
33. Mittal, A., Soundararajan, R., Bovik, A.C.: Making a “completely blind” image quality analyzer. IEEE SPL (2012)
34. Nah, S., Son, S., Lee, J., Lee, K.M.: Clean images are hard to reblur: Exploiting the ill-posed inverse task for dynamic scene deblurring. In: ICLR (2022)
35. Online: Flickr2k. <https://www.flickr.com/>, accessed: 20204-03-05
36. Potlapalli, V., Zamir, S.W., Khan, S., Khan, F.S.: Promptir: Prompting for all-in-one blind image restoration. arXiv:2306.13090 (2023)
37. Qu, Y., Chen, Y., Huang, J., Xie, Y.: Enhanced pix2pix dehazing network. In: CVPR (2019)
38. Ren, C., He, X., Wang, C., Zhao, Z.: Adaptive consistency prior based deep network for image denoising. In: CVPR (2021)
39. Ren, W., Liu, S., Zhang, H., Pan, J., Cao, X., Yang, M.H.: Single image dehazing via multi-scale convolutional neural networks. In: ECCV (2016)
40. Ren, W., Pan, J., Zhang, H., Cao, X., Yang, M.H.: Single image dehazing via multi-scale convolutional neural networks with holistic edges. IJCV (2020)
41. Ridnik, T., Ben-Baruch, E., Noy, A., Zelnik-Manor, L.: Imagenet-21k pretraining for the masses. arXiv:2104.10972 (2021)
42. Schuhmann, C., Beaumont, R., Vencu, R., Gordon, C., Wightman, R., Cherti, M., Coombes, T., Katta, A., Mullis, C., Wortsman, M., et al.: Laion-5b: An open large-scale dataset for training next generation image-text models. NeurIPS (2022)
43. Talebi, H., Milanfar, P.: Nima: Neural image assessment. TIP (2018)
44. Tian, C., Xu, Y., Zuo, W.: Image denoising using deep cnn with batch renormalization. Neural Networks (2020)
45. Tsai, F.J., Peng, Y.T., Tsai, C.C., Lin, Y.Y., Lin, C.W.: BANet: A blur-aware attention network for dynamic scene deblurring. TIP (2022)
46. Tu, Z., Talebi, H., Zhang, H., Yang, F., Milanfar, P., Bovik, A., Li, Y.: MAXIM: Multi-axis MLP for image processing. In: CVPR (2022)
47. Wang, Z., Cun, X., Bao, J., Liu, J.: Uformer: A general u-shaped transformer for image restoration. arXiv:2106.03106 (2021)
48. Wei, W., Meng, D., Zhao, Q., Xu, Z., Wu, Y.: Semi-supervised transfer learning for image rain removal. In: CVPR (2019)
49. Xie, W., Song, D., Xu, C., Xu, C., Zhang, H., Wang, Y.: Learning frequency-aware dynamic network for efficient super-resolution. In: ICCV (2021)

50. Yang, F., Yang, H., Fu, J., Lu, H., Guo, B.: Learning texture transformer network for image super-resolution. In: CVPR (2020)
51. Yasarla, R., Patel, V.M.: Uncertainty guided multi-scale residual learning-using a cycle spinning cnn for single image de-raining. In: CVPR (2019)
52. Zamir, S.W., Arora, A., Khan, S., Hayat, M., Khan, F.S., Yang, M.H.: Restormer: Efficient transformer for high-resolution image restoration. In: CVPR (2022)
53. Zamir, S.W., Arora, A., Khan, S., Hayat, M., Khan, F.S., Yang, M.H., Shao, L.: CycleISP: Real image restoration via improved data synthesis. In: CVPR (2020)
54. Zamir, S.W., Arora, A., Khan, S., Hayat, M., Khan, F.S., Yang, M.H., Shao, L.: Multi-stage progressive image restoration. In: CVPR (2021)
55. Zhang, H., Patel, V.M.: Density-aware single image de-raining using a multi-stream dense network. In: CVPR (2018)
56. Zhang, K., Danelljan, M., Li, Y., Timofte, R., Liu, J., Tang, J., Wu, G., Zhu, Y., He, X., Xu, W., et al.: AIM 2020 challenge on efficient super-resolution: Methods and results. In: ECCV Workshops (2020)
57. Zhang, K., Zuo, W., Chen, Y., Meng, D., Zhang, L.: Beyond a gaussian denoiser: Residual learning of deep cnn for image denoising. TIP (2017)
58. Zhang, K., Zuo, W., Gu, S., Zhang, L.: Learning deep CNN denoiser prior for image restoration. In: CVPR (2017)
59. Zhang, K., Zuo, W., Zhang, L.: Ffdnet: Toward a fast and flexible solution for cnn-based image denoising. TIP (2018)
60. Zhang, K., Luo, W., Zhong, Y., Ma, L., Stenger, B., Liu, W., Li, H.: Deblurring by realistic blurring. In: CVPR (2020)
61. Zhao, H., Gou, Y., Li, B., Peng, D., Lv, J., Peng, X.: Comprehensive and delicate: An efficient transformer for image restoration. In: CVPR (2023)
62. Zhou, M., Huang, J., Guo, C.L., Li, C.: Fourmer: An efficient global modeling paradigm for image restoration. In: ICLR (2023)

Supplemental Material

Here, we have discussed the details about the transformer block used in our DyNet, additional sample images from our Million-IRD dataset, additional visual results comparison between PromptIR [36] and the proposed DyNet-L in all-in-one setting.

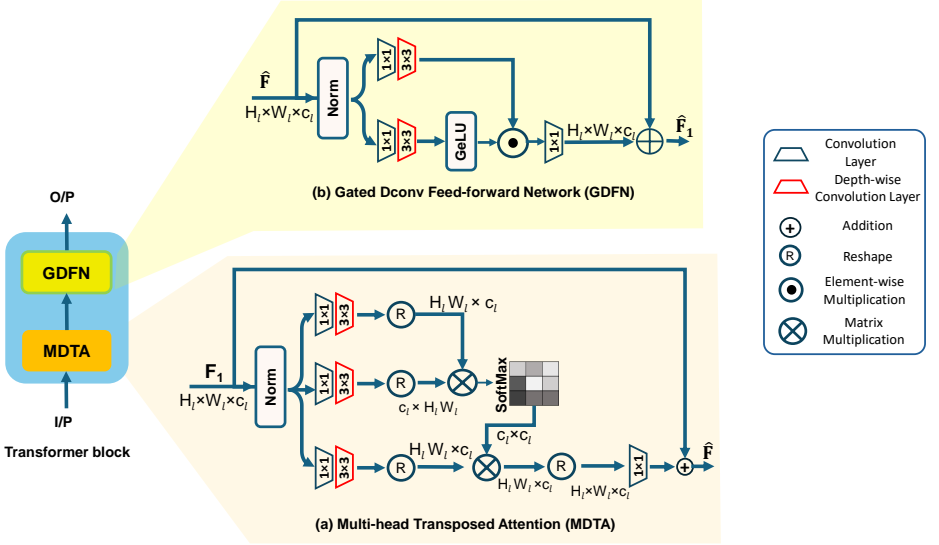


Fig. S1: Overview of the Transformer block used in our DyNet network. The Transformer block is composed of two sub-modules, the Multi Dconv head transposed attention module (MDTA) and the Gated Dconv feed-forward network (GDFN).

A Transformer Block Details

As described in Section 3.1 of the main manuscript, here, we have discussed the transformer block utilized within our DyNet network architecture, detailing its sub-modules multi deconv head transposed attention (MDTA) and gated deconv feed-forward network (GDFN). Initially, input features, represented as $R \in H_l \times W_l \times C_l$, are processed through the MDTA module. Within this, Layer normalization is used to normalize the input features. This is followed by the application of 1×1 convolutions and then 3×3 depth-wise convolutions, which serve to transform the features into Query (Q), Key (K), and Value (V) tensors. A key feature of the MDTA module is its focus on calculating attention across the channel dimensions, instead of the spatial dimensions, which significantly reduces computational demands. For channel-wise attention, the Q and K tensors are reshaped from $H_l \times W_l \times C_l$ to $H_l W_l \times C_l$ and $C_l \times H_l W_l$ dimensions,

respectively. This reshaping facilitates the computation of the dot product and leads to a transposed attention map of $C_l \times C_l$ dimensions. This process incorporates bias-free convolutions and executes attention computation simultaneously across multiple heads. Following the MDTA Module, the features undergo further processing in the GDFN module. Within this module, the input features are initially expanded by a factor of γ through the use of 1×1 convolutions. Subsequently, these expanded features are processed with 3×3 convolutions. This procedure is executed along two parallel pathways. The output from one of these pathways is subjected to activation through the GeLU non-linear function. The activated feature map is then merged with the output from the alternative pathway via an element-wise multiplication.

B Visual Results Comparison

We show additional visual results comparison between PromptIR [36] and our DyNet-L under from all-in-one setting.



Fig. S2: Comparative analysis of image denoising by all-in-one methods on the BSD68 dataset [30]. Our DyNet-L reduces noise, producing more sharp and clear image compared to the PromptIR [36].



Fig. S3: Comparative analysis of image deraining by all-in-one methods on the Rain100L dataset [16]. Our DyNet-L successfully eliminates rain streaks, producing clear, rain-free images as compared to the recent PromptIR [36].



Fig. S4: Comparative analysis of image dehazing by all-in-one methods on the SOTS dataset [25]. Our approach reduces haze, producing more clear image compared to the PromptIR [36].

Table S1: Overview of the number of images curated from each database for our Million-IRD dataset.

Dataset	NTIRE [4]	DIV2K [2]	Flickr2K [35]	LSDIR [27]	Laion-HR [42]
#Images	56	2,000	2,000	84,991	2M



Fig. S5: Sample images from our Million-IRD dataset, which features a diverse collection of high-quality, high-resolution photographs. This includes a variety of textures, scenes from nature, sports activities, images taken during the day and at night, intricate textures, wildlife, shots captured from both close and distant perspectives, forest scenes, pictures of monuments, etc.

C Breakdown of images in Our Million-IRD Dataset

We combine the existing high-quality, high-resolution natural image datasets such as LSDIR [27], DIV2K [2], Flickr2K [35], and NTIRE [4]. Collectively these datasets have 90K images having spatial size ranging between $< 1024^2, 4096^2 >$. Their breakdown is given in Table S1. We also show the additional sample images from our Million-IRD dataset in Fig. S5 and Fig. S6.

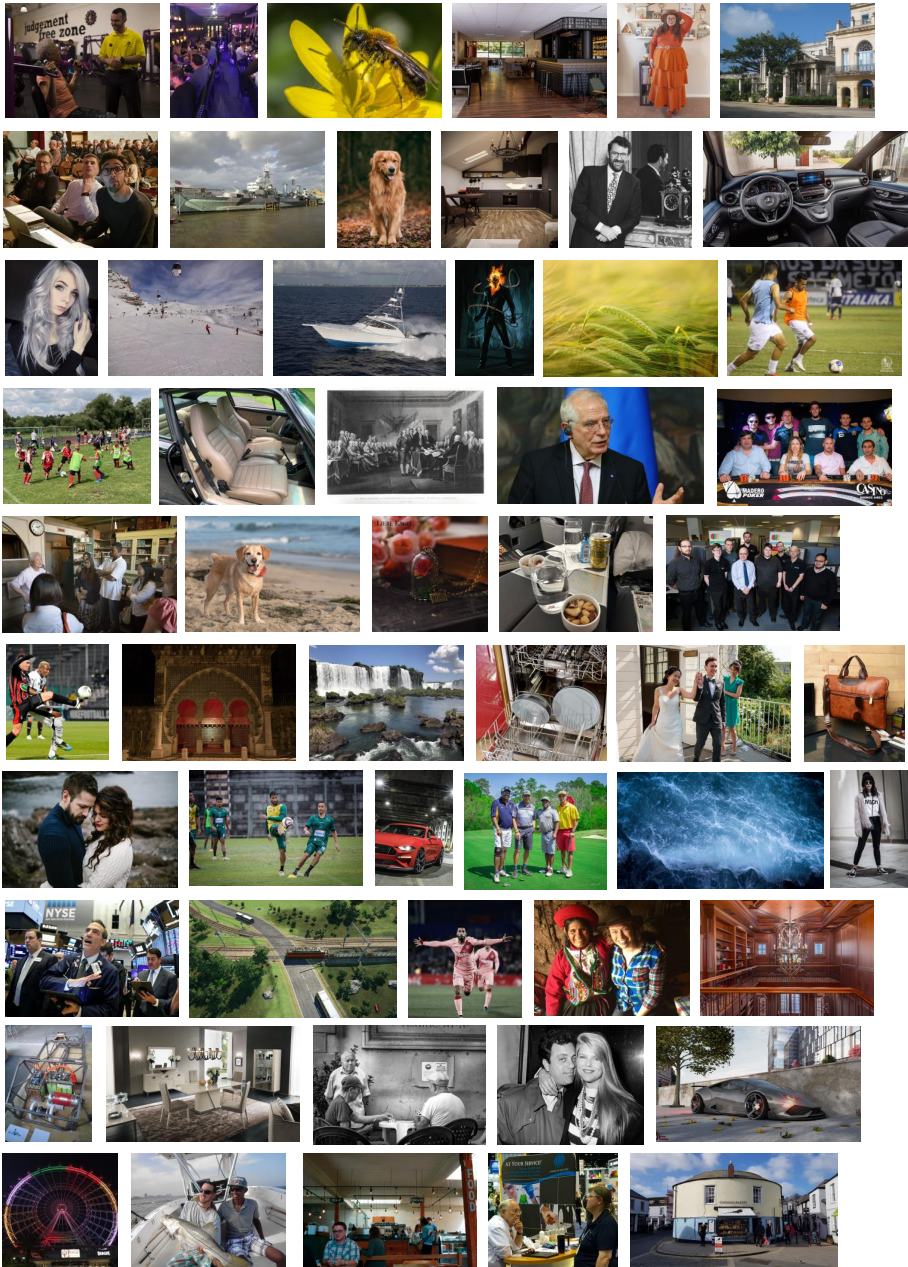


Fig. S6: Sample images from our Million-IRD dataset, which features a diverse collection of high-quality, high-resolution photographs. This includes a variety of textures, scenes from nature, sports activities, images taken during the day and at night, intricate textures, wildlife, shots captured from both close and distant perspectives, forest scenes, pictures of monuments, etc.